OMI Level 0 to 1b Processing and Operational Aspects

G. H. J. van den Oord, Nico C. Rozemeijer, V. Schenkelaars, Pieternel F. Levelt, Marcel R. Dobber, Robert H. M. Voors, J. Claas, Johan de Vries, M. ter Linden, C. De Haan, and T. van de Berg

***Abstract*—The Ozone Monitoring Instrument (OMI) was launched on July 15, 2004 on the National Aeronautics and Space Administration's Earth Observing System Aura satellite. OMI is an ultraviolet-visible imaging spectrograph providing daily global coverage with high spatial resolution. This paper discusses the ground data processing software used for Level 0 to Level 1b processing of OMI data. In addition, the OMI operations scenario is described together with the data processing concept. This paper is intended to serve as a reference guide for users of OMI (Level 1b) data.**

***Index Terms*—Data management, data processing, remote sensing, ultraviolet spectroscopy.**

I. Introduction

THE Ozone Monitoring Instrument (OMI) was launched on board the Earth Observing System (EOS) Aura satellite on July 15, 2004. The OMI instrument is a nadir-viewing ultraviolet-visible (UV-VIS) imaging spectrometer providing daily global coverage with high spatial and spectral resolution. The scientific objectives of the OMI instrument are described in [1], and a full instrument description can be found in [2] and a brief description in [3]. In this paper, we describe the software that is used to process raw instrument data (Level 0 data) to calibrated measurement data (Level 1b data). This software is commonly referred to as the ground data processing software (GDPS). The GDPS is developed by Dutch Space and is commissioned by the Netherlands Agency for Aerospace Programs (NIVR). The scientific responsibility resides at the Royal Netherlands Meteorological Institute (KNMI). The GDPS development has been a rather unique process because of the way the OMI Program is organized: Instrument Operations, Instrument Calibration, and GDPS development fall under the responsibility of one organization (KNMI). This allowed effective communication across a number of important interfaces resulting in a flexible development. As a result, the GDPS has been flawlessly processing OMI data from launch onward and even during the on-ground satellite testing. Each 100-min orbit OMI produces about 0.5-GB Level 0 data that is processed by the GDPS into 1–1.5-GB Level 1b data.

Manuscript received May 20, 2005; revised September 23, 2005. This work was supported by the Netherlands Agency for Aerospace Programmes (NIVR).

G. H. J. van den Oord, P. F. Levelt, M. R. Dobber, R. Voors, and J. Claas are with the Royal Netherlands Meteorological Institute (KNMI), 3730 AE De Bilt, The Netherlands (e-mail: oordvd@knmi.nl).

V. Schenkelaars, J. de Vries, M. ter Linden, C. de Haan, and T. van de Berg are with Dutch Space, 2303 DB Leiden, The Netherlands.

N. C. Rozemeijer is with TriOpSys BV, 3605 JW Maarsen, The Netherlands.

Digital Object Identifier 10.1109/TGRS.2006.872935

There were a number of important design drivers for the GDPS. First, the high data rate of OMI and second the almost infinite ways in which the instrument can be programmed for readout. The former implied that very robust software with a good performance had to be developed and the latter that the software needed to be able to handle all possible instrument configurations. A third design driver was that OMI performs different types of measurements for different groups of users: radiance and irradiance measurements are used for Level 2 product generation while calibration and irradiance measurements are used by calibration scientists. Each of these user groups has specific needs, and these are accommodated by the GDPS in the form of various output products. In order to be able to discuss the impact of these design drivers we discuss in Section II, the operations and data processing concept of the OMI instrument. In Section III, the development and some aspects of the architecture of the GDPS are discussed. In Section IV, a forward model of the signal flow through the OMI instrument is presented, and in Section V this model is inverted and discussed in terms of the actual correction algorithms implemented in the GDPS. Section VI focuses on the flagging and the flag-related metadata in the GDPS output products. Conclusions are presented in Section VII.

This paper is intended to serve as a comprehensive reference guide for users of OMI (Level 1b) data in combination with [2] and [6]. It also serves to demonstrate the integrated approach between data processing, instrument operations, and calibration that has been implemented for OMI.

II. Operations and Data Processing Concept

A. Instrument Operations Concept

The Aura satellite has an orbital period of 98.9 min at an inclination of 98.2° and an altitude of 705 km. On the day side of the orbit OMI performs radiance measurements (in short EARTH) and on the night side calibration measurements. These calibration measurements consist of White Light Source (WLS) measurements, LED measurements (LED), and dark current (DARK) measurements [2]. Near the North Pole, irradiance measurements (SUN) are performed at a daily, weekly, and monthly frequency depending on the diffuser that is used [2]. EARTH, SUN, WLS, LED, and DARK are referred to as *MeasurementClasses*. In the GDPS, each MeasurementClass has its own processing flow in terms of corrections applied to the measurements. OMI allows a very flexible readout based on parameters like Master Clock Period, exposure time, binning factors, gain switch columns, gain values, and row skip values

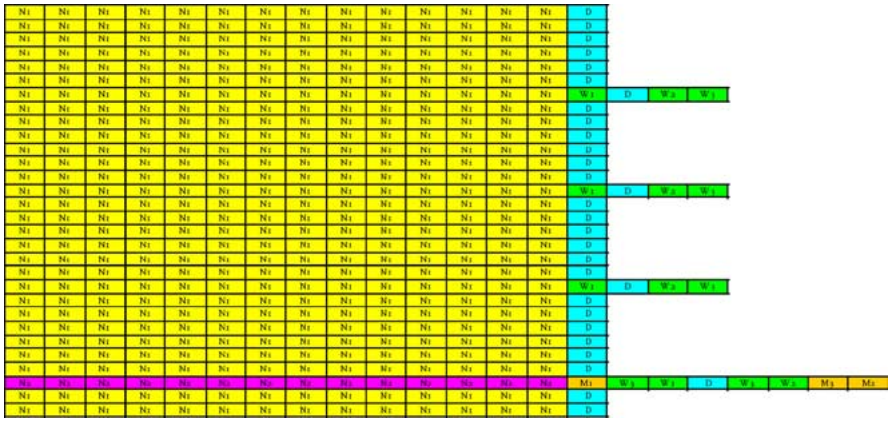

Fig. 1. Operations baseline for OMI based on the orbital repeat cycle of Aura (466 orbits). Each horizontal line corresponds to roughly one day of 15 orbits except once per week when the weekly orbits (green) are executed. One day per month OMI performs spatial zoom-in measurements (purple N2 orbits) and also the monthly orbits (orange) are executed.

[2]. A baseline has been defined of 178 specific instrument settings that are referred to as *measurement types*. Each measurement type has an associated Instrument Configuration Identifier (IcId) and a version number. An important aspect of the operations concept is that for each measurement type of MeasurementClass EARTH, SUN, WLS, and LED, an accompanying dark measurement is performed in the same orbit.

The measurement types constitute the building blocks of the OMI operations. At the higher level a total number of nine types of orbits have been defined with the following names: Nominal 1 (N1), Nominal 2 (N2), Daily (D), Weekly 1 (W1), Weekly 2 (W2), Weekly 3 (W3), Monthly 1 (M1), Monthly 2 (M2), and Monthly 3 (M3). Each orbit type consists of a fixed sequence of measurement types. The Appendix provides a list of all measurement types, their IcId and MeasurementClass, and the orbit types in which they are executed. A number of measurement types were only used during the launch and early operations phase of the mission for the purpose of instrument check-out and in-flight calibration.

At the next higher level the orbit types are executed in a specific sequence with a periodicity of 466 orbits. The latter coincides with twice the orbital repeat cycle of the Aura satellite. This operations schedule is shown in Fig. 1. One orbit per month when the M3 orbit is executed, which contains only dark measurements, OMI does not perform radiance measurements. Also, one day per month OMI performs spatial zoom measurements (N2 and M1 orbits). Because of the orbital repeat cycle these always cover the same groundtracks. All other days OMI performs global measurements on the day side of the orbit resulting in global coverage. OMI observes standard 60 groundpixels (13 km $\times$ 24 km) across the swath in the UV2 (307–383 nm) and VIS (349–504 nm) channels and 30 groundpixels (13 km $\times$ 48 km) in UV1 (264–311 nm). For spatial zoom measurements these numbers remain the same but both the total swath width and the groundpixel size are reduced by a factor two [2].

The most frequently executed orbit is the Nominal 1 orbit. The measurement types for this orbit are the Global Arctic, Global Midlattitude, and Global Tropical and their accompanying darks. These measurement types only differ in the gainswitching and exposure times (and hence the number of co-additions) that are applied to accommodate variations in the radiance levels along the orbit. During the ozone hole "season" the global Arctic is, near the South Pole, replaced by a global ozone hole measurement type that is optimized for measuring ozone hole radiances by changing the so-called gainswitch columns on the charge-coupled device (CCD). The net effect is that the signal amplification in the UV1 channel is reduced in order to avoid saturation by the increased radiance levels during ozone hole conditions.

TABLE I
MEASUREMENT CLASSES OF OMI AND THE RELATED OUTPUT PRODUCTS

Measument Class	Product Shortname	Product description
EARTH	OML1BRUG	Global radiances UV channel
	OML1BRVG	Global radiances VIS channel
	OML1BRUZ	Zoom radiances UV channel
	OML1BRVZ	Zoom radiances VIS channel
	OML1BCAL	Calibration product
SUN	OML1BIRR	Irradiances UV &VIS channel
	OML1BCAL	Calibration product
WLS	OML1BCAL	Calibration product
LED		
DARK		

OMI flies from south to north on the dayside. The switching between different measurement types along the orbit is a function of orbital phase. This makes OMI operations independent of season. For example, for the N1, D, W1, W2, W3, M2 orbit types, the sequence for the dayside part is as follows: arctic, midlatitude, tropical, midlatitude, and arctic. The operational scenario has been optimized to provide consistent and uninterrupted science data.

B. Data Processing Concept

In the previous section we discussed the concept of MeasurementClass and its relation to the operations scenario. In addition to each MeassurementClass having its own processing flow in the GDPS, the results are written in separate output products. For OMI six output products have been defined. Their relation to each MeasurementClass is given in Table I in which the so-called product shortnames are used. The filename convention for OMI Level 1b products follows that for Aura. It consists of a instrument/platform/product-level identifier,

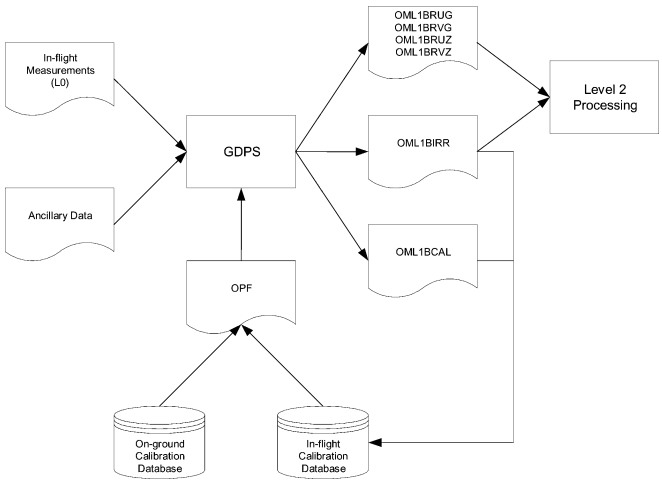

Fig. 2. Data processing concept for the GDPS. The GDPS ingests OMI measurements, ancillary data (attitude and ephemeris, snow-ice maps) and calibration constants from the OPF. The OPF is fed from the on-ground and in-flight calibration databases. The in-flight calibration database is fed from the irradiance and the calibration product. Radiance products and the irradiance product are used for further processing to Level 2 data products.

the product shortname, measurement date-time, orbit number, ECS collection version number and production date-time. Each product file (granule) starts at spacecraft midnight and contains one orbit worth of data. The measurement date-time in the filename is the time of spacecraft midnight at the start of the granule. The ECS collection version number indicates the release version of OMI data. An example file name is OMI-Aura_L1-OML1BRUG_2005m0511t1648-o04375_v002-2005m0512t172 006.he4. Files are based on the HDF-EOS 2.x format and make use of so-called swath datasets.

The way in which the GDPS ingests and outputs data has been an important design driver for the ground segment. In Fig. 2 the functional data flow is shown. The GDPS ingests Level 0 data from the instrument, attitude and ephemeris data for the spacecraft (also called DPREP) and ancillary data like NISE snow-ice maps. Another important input file is the so-called Operational Parameter File (OPF) that contains all calibration constants needed for processing. This file is fed from the on-ground and in-flight calibration databases. The latter is in turn fed from the information in the OML1BCAL and OML1BIRR products. In this way it is possible to maintain the in-flight calibration. The operational concept guarantees that all required measurements are performed that are needed to track the instrument performance and to accommodate instrument changes in the calibration constants. Whenever a calibration measurement is not available it can be rescheduled depending on its importance. A measurement can be missed because of, for example, spacecraft maneuvers. However, spacecraft maneuvers are normally scheduled at times that do not conflict with the most important OMI calibration measurements.

The actual processing is spread over a number of facilities in the U.S., The Netherlands, and Finland. These facilities are the OMI Science Investigator-led Processing System (OMI-SIPS), the OMI Dutch Processing System (ODPS), the Trend Monitoring and Calibration Facility (TMCF), and the Sodankyla Receiving Station. OMI data products are stored in the Goddard

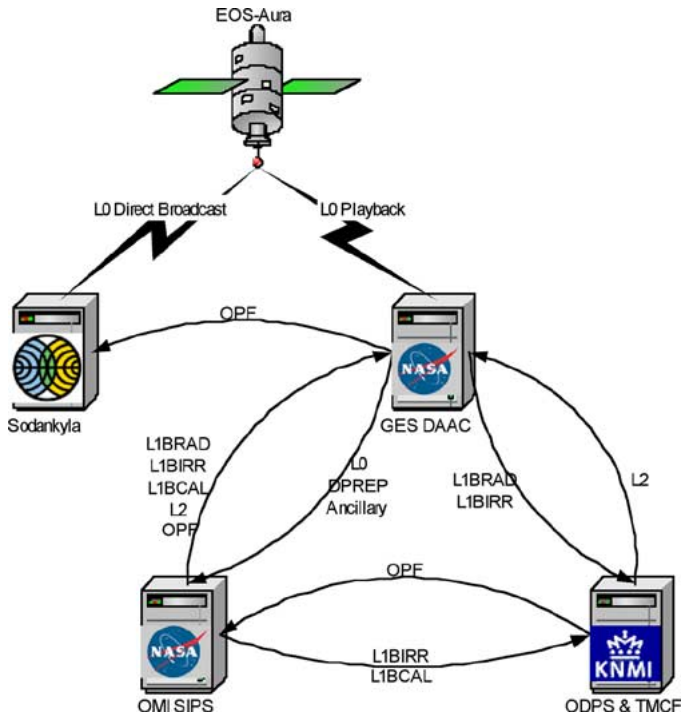

Fig. 3. Layout of the OMI ground segment showing the data products that are exchanged. The facilities are spread over the U.S. (OMI SIPS and GES-DAAC), The Netherlands (ODPS and TMCF), and Finland (Sodankyla). The OMI instrument on that Aura spacecraft generates Level 0 (L0) data. These are down-linked and send to the GES-DAAC. The GES-DAAC ships these data together with attitude and ephemeris data (DPREP) and Ancillary data to the OMI SIPS where they are processed to Level 1b and Level 2 (L2) data products. These are shipped to the GES-DAAC and the ODPS/TMCF where they are used for Level 2 product generation (ODPS) and calibration purposes (TMCF). The TMCF updates the OPF that is shipped to the OMI SIPS that forward it to the GES-DAAC. The GES-DAAC forward it then to the Sodankyla processing system.

Earth Science Distributed Active Archive Center (GES-DAAC). The OMI-SIPS produces Level 1b and Level 2 products, while the ODPS only produces Level 2 products. The Sodankyla station produces Very Fast Delivery Level 2 products for Northern Europe based on Direct Broadcast data from the Aura spacecraft. Both higher level products and Near Real Time products will be available in the near future.

The high data rate of OMI, in combination with the large numbers of instrument configurations and calibration constants, makes it impossible to maintain the in-flight calibration without resorting to automation. For that purpose the TMCF was developed. This facility produces a large number of special calibration products, based on OML1BCAL and OML1BIRR that can be used to trend the calibration constants. A number of these products can be directly inserted into the OPF.

Fig. 3 shows the various processing facilities and the products that are exchanged. OMI standard data products are made available for users via the GES-DAAC that provides various tools and means to access the data. Data consistency is maintained by having all processing centers using identical Operational Parameter Files and identical versions of the software. The OMI Configuration Tracking Board checks that these conditions are met. Whenever an OPF is not available forward processing is halted except for the Near Real Time production that continues with the

most recent OPF that is available. For reprocessing campaigns all OPFs and software that are required are first staged before the actual reprocessing starts.

III. Development and Architecture of the GDPS

The GDPS was developed by Dutch Space according to the PSS-05-lite standard [4]. This standard defines a User Requirements phase, a Software Requirements/Architectural Design phase, a Detailed Design and Production phase and a Transfer phase. Formal, external reviews are an integral part of these development phases. The approach is evolutionary in the sense that at each milestone all requirements are again reviewed. The milestones for the GDPS were: the User Requirement Review (July 1999), Software Requirements/Architectural Design Review (April 2000), Detailed Design Review (May 2001), Provisional Acceptance Reviews (June 2002, May 2003), and the Final Acceptance Review (December 2004). This schedule was mainly driven by the foreseen launch date of Aura that slipped on various occasions.

The software development process involved three parties, each with their own responsibilities. A science team that was responsible for drafting and developing the science algorithms; a software team consisting of software engineers for the design of the software and implementation of the algorithms and an independent test team responsible for the verification of the software. The validation of the software was a joint responsibility of the science team and the test team. This approach combines the best of both science and engineering worlds, and has led to very robust, high-quality software with scientifically correct functionality.

A lot of effort was spent on verification and validation of the software. There is an important difference between software verification and validation. For an instrument, or its properties, a physical model can be constructed. Verification serves to test whether the model is correctly implemented in the software. Validation serves to check whether the model is a correct representation of the instrument properties.

The verification of the GDPS consisted of three levels of testing, Unit tests, Integration tests and System and Acceptance tests, each with a high level of automation. Additionally, independent code reviews were held and third party test tools were used for detecting problems related to memory leaks and memory corruption and for measuring test coverage.

Starting about a year before launch, the GDPS was used in a large number of ground system end-to-end tests. These consisted of so-called Mission Operational Science Simulations during which OMI data were played-back at the polar ground stations. The data flowed through the ground segment and were processed by the OMI SIPS and the ODPS up to and including Level 2 products. Another type of end-to-end test was performed during on-ground testing of the spacecraft when instrument data were also pushed through the ground system and processed.

It is not possible to describe the GDPS architecture in full detail but three of the various main components are: the Preparator, the Processor and the Output Generator. The Preparator reconstructs the images that have been measured from the engineering telemetry and the video data of the UV and VIS channel. An important feature of the Preparator is that it hides as much of the instrument's complexity as possible. This allows the algorithms, which are the most subject to change, to be developed in a generic, more straightforward manner.

The component Processor processes the images containing the instrument data into physical quantities like radiances, irradiances and calibration data. This occurs in a pipeline fashion in the sense that sequential measurements are sequentially processed and are considered to be independent. The algorithms used are discussed in Section V. The third component is the Output Generator that generates the output products and the metadata.

It is possible to use the GDPS in combination with a Level 0 Preprocessor (L0PP). This L0PP can be used to reformat data from various sources into a format that can be ingested by the GDPS. The L0PP is capable of removing artifacts, such as duplicate and out-of-order data from the Level 0 data stream. It has been used for processing raw telemetry from the satellite, on-ground calibration measurements, data from an instrument simulator, and data from a Test Data Generator.

IV. Forward Model

In this section a forward model for the signal flow through the instrument is presented. This forward model serves as a guide for the inverse model discussed later.

OMI can be considered as a system with four components: a telescope, a spectrograph, a detector, and readout electronics.

In the following a systematic description is given of all four elements, in terms of the signal flow through each element.

A. Telescope

There are three different ways in which light can pass through the OMI telescope (see [2, Fig. 1]).

1) Light can enter the telescope through the nadir port, through aperture (001), is then reflected off the primary mirror (103), goes through the scrambler (005) and is then focused by the secondary mirror (007) on the spectrograph slit (008).
2) Light can enter via the sun port, passes through the mesh, then falls on one of the three reflection diffusers, is reflected off the folding mirror C03 toward the scrambler, from where it follows the same path as light that enters through the nadir port.
3) Light from the onboard White Light Source is reflected off mirror C10, transmitted through the transmission diffuser C05 and after reflection off the folding mirror C03 follows the same path as that of a solar light beam.

These three different light paths result in three different descriptions of the signal that is incident on the spectrograph slit S_{slit} (in photons per second per radian per nanometer).

Radiance measurement:

$$S_{\text{slit}}(\lambda,\alpha,t)=S_{\text{earth\_radiance}}(\lambda,\alpha,P,t)R_{\text{tel\_earth}}(\lambda,\alpha) \quad (1a)$$

Irradiance measurement:

$$S_{\text{slit}}(\lambda,\alpha) = S_{\text{solar-irradiance}}(\lambda) \times \text{BRDF}(\lambda,\alpha) R_{\text{tel\_sun}}(\lambda,\alpha) \tag{1b}$$

WLS measurement:

$$S_{\text{slit}}(\lambda,\alpha) = S_{\text{wls}}(\lambda,\alpha) R_{\text{tel\_WLS}}(\lambda,\alpha) \tag{1c}$$

Here, λ is the wavelength, α is the viewing direction (the swath angle), P is the polarization state of the incident light, t is time, and $\text{BRDF}(\lambda,\alpha)$ is the Bidirectional Reflection Distribution function of an internal diffuser. The different R indicate the specific throughputs of the different optical paths. A key design element in OMI is the choice to have the primary mirror made of the same material as the folding mirror so that $R_{\text{tel\_earth}}$ is equal to $R_{\text{tel\_sun}}$ apart from a factor related to the mesh in the irradiance light path. The throughput functions are independent of polarization state of the incident light because of the polarization scrambler, and a design property of the first scrambler surface that serves to compensate to a large extent for polarization effects induced by the primary mirror.

For radiance observations, the nadir direction is imaged at the center of the spectrograph slit and the extreme swath angles at the edges of the slit. For irradiance observations, the slit receives light from different parts of the diffuser, as a function of position along the slit.

B. Spectrograph

The spectrograph projects an image of the slit on the detector while dispersing the signal in the spectral direction. This can be described by a multiplication with the throughtput-function of the specific channel optics ($R_{\text{channel\_optics}}$ for UV-1, UV-2 , and VIS) and a convolution with the slit function (r_{chan})

$$S_{\text{useful}}(\lambda,\alpha,t) = \int_0^\infty S_{\text{slit}}(\lambda',\alpha,t) R_{\text{channel\_optics}}(\lambda') \times \rho(\alpha) r_{\text{chan}}(\lambda-\lambda',\alpha) d\lambda'. \tag{2}$$

Note that each (sub)channel has its proper slit function as is reflected in the different spectral resolutions. The slit function also varies as a function of swath angle α. The entrance slit of the spectrograph has small irregularities along the slit due to manufacturing limitations. These are captured by the function $\rho(\alpha)$.

Unwanted internal reflections (e.g., from the grating) will cause out-of-band (spectral) and/or out-of-field (spatial) stray light. The amount of stray light scales with the amount of useful light, often in a very complex way [2]. Symbolically, we can write

$$S_{\text{total}} = S_{\text{useful}} + S_{\text{straylight}}(S_{\text{useful}}). \tag{3}$$

C. Charge Generation on the CCD

The photon field incident on the detector is now given by $S_{\text{total}}(\lambda,\alpha,t)$. Let (x,y) be a coordinate system on the CCD with the centres of the CCD pixels located on a grid (x_i,y_j). We can write $x = f(\lambda,\alpha)$ and $y = g(\lambda,\alpha)$ with f and g functions that provide the mapping between CCD coordinates and wavelength and viewing direction. In the ideal case each CCD pixel column would correspond to a specific wavelength and each CCD pixel row to a specific viewing angle (so $x = f(\lambda)$ and $y = g(\alpha)$). OMI has, however, a clear spectral smile and also a small spatial smile.

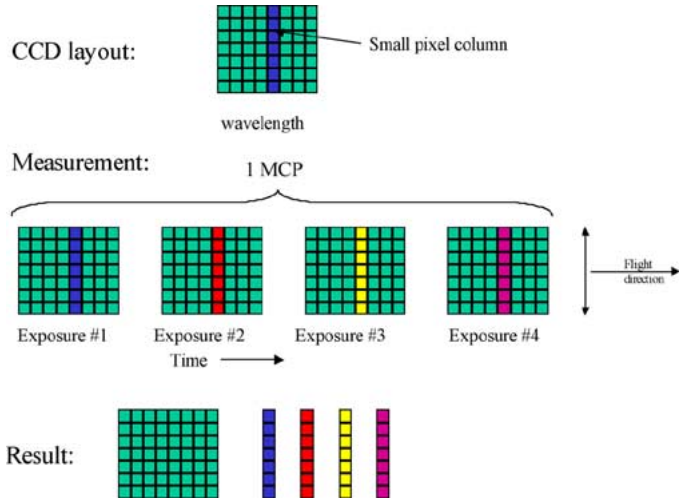

Fig. 4. Concept of small pixel data. The middle of the figure shows the measurement: four consecutive exposures are performed, each at a different time. The four exposures are, onboard, digitally co-added but the four measured small pixel columns (dark blue, red, yellow, purple) are kept apart. The Level 0-1b processor combines the four small pixel columns and generates a complete image for one MCP but also outputs the four measured small pixel columns separately in the Level 1b product. The result is shown at the bottom of the figure. The process of row binning is not shown in the figure. It occurs automatically when each of the four exposures is read out. In this example the number of co-additions is four but it can equally be five, two or one. The number of small pixel columns will vary accordingly.

The sensitivity of CCD pixel (i,j) is a function of the pixel response function (PRF) of that pixel $\text{PRF}(i,j\,|\,x,y)$. To calculate the number of electrons generated in a pixel we have to integrate the photon field multiplied by the pixel response function over the surface area of the pixel

$$\begin{aligned} S_{\text{electrons}}(i,j,t) &= \iint S_{\text{total}}(\lambda,\alpha,t) \cdot \text{PRF}(i,j\,|\,x,y) \cdot dx \cdot dy \\ &= \iint S_{\text{total}}(\lambda,\alpha,t) \cdot \text{PRF}(i,j\,|\,\lambda,\alpha) \\ &\quad \times\ J(x,y\,|\,\lambda,\alpha) d\lambda d\alpha \end{aligned} \tag{4}$$

with $J = f_\alpha g_\lambda - f_\lambda g_\alpha$ the Jacobian accounting for the curved projection of the photon field on the rectangular CCD pixel grid. The typical full-widths at half-maximum of a PRF in the two relevant CCD directions determine the spectral and spatial sampling distances of a pixel. These set the effective integration limits in the above integral.

The photons incident on a CCD pixel create free electrons at a rate proportional to the quantum efficiency. It is possible to write the pixel response function PRF as a dimensionless normalized PRF times the quantum efficiency (QE) of that pixel. For practical purposes it is useful to write the quantum efficiency of a pixel as the average quantum efficiency of the CCD at the typical wavelength of the pixel times a pixel-specific pixel response nonuniformity (PRNU)

$$\text{QE}(i,j,) = \overline{\text{QE}}(\lambda) \cdot \text{PRNU}(i,j,). \tag{5}$$

By combining (1)–(5) we can (symbolically) write

$$S_{\text{electrons}}(i,j) = \langle S_{\text{input}} \rangle \text{PRNU}(i,j)\rho(i)\Re(i,j)t_{\text{exp}}. \quad (6)$$

In this expression, $\langle S_{\text{input}} \rangle$ is the (radiance, irradiance, or WLS) input spectrum at OMI resolution, ρ is the slit irregularity and $\Re$ is the appropriate response function. This function contains the throughput along an optical path and the average quantum efficiency. Note that in (6) we have multiplied with the exposure time t_{exp}.

A second source of charge generation in a pixel is dark current. The amount of dark current is a simple function of temperature and doubles, roughly, every 5 K. The temperature behavior of the dark current has been characterized both on-ground and in-flight over a temperature range of 263–303 K. During nominal operations the (actively controlled) CCD temperature is constant within 10 mK. The operations scenario guarantees that for every measurement (SUN, EARTH, WLS, LED) a corresponding dark measurement is performed resulting in an optimal dark current characterization. For the OMI CCDs there is only a very slight difference between the dark current distributions in the image area and in the (masked) storage area.

D. CCD Readout

The OMI CCDs are frame-transfer CCDs and a discussion of the transfer of charges is facilitated by using the picture of parcels of electrons travelling over a fixed grid of CCD pixels. In each pixel, in which a parcel resides for some time, the amount of electrons contained in the parcel changes due to illumination by photons and/or dark current. The transfer of a parcel over the CCD occurs in six steps.

- Step 1) Rapid transfer of the parcel from the top of the CCD to the pixel location in the image area where the exposure takes place.
- Step 2) Exposure to "useful" signal (actual measurement of duration t_{exp}).
- Step 3) Rapid transfer from image region to corresponding location in storage region.
- Step 4) (Slow) vertical transfer through storage region, toward the read-out register.
- Step 5) Transfer of the parcel into read-out register. Multiple parcels, that is, multiple CCD rows, are added in the read-out register (binning).
- Step 6) Horizontal transfer through the read-out register toward the output capacitance at which the charge content of a parcel is measured in terms of a voltage over the capacitance.

During each of these steps the dark current contribution to a parcel increases proportional to the time the parcel spends in a specific pixel and the (typical) dark current of that pixel.

During Steps 1) and 3), the parcel moves rapidly over the image area of the CCD. Because this area is illuminated during these transfers, additional charge is added to the parcel. This additional charge is called the *smear signal*. For a constant illumination it corresponds to the integrated signal along a CCD column times the ratio of the frame transfer time over the exposure time. Furthermore, the image areas of the OMI CCDs have a few masked rows at the top of the CCDs and near the storage area. The parcels that have their useful exposure [Step 2)] in these masked pixels contain in the end only information about the smear signal (in addition to dark current signal). This information can also be used for correction of the smear effect. When a parcel moves to the next pixel a tiny fraction of the charge in the parcel is left behind. At the same time the parcel picks up some charges left behind by the preceding parcel. This effect is related to the charge transfer efficiency (CTE) of the CCD pixels. For the OMI CCDs less than 1% (on average about 0.5–0.7%) of charge injected at the top of a CCD does not arrive at the output capacitance. For charges injected in the lower part of the image area the amount of charge left behind is even less. Because the charge in a parcel changes continuously, because of illumination and/or dark current, modeling of CTE effects involves considerable bookkeeping.

Both numerical and analytical models have been developed in the OMI project to describe CTE effects on the useful signal, on the smear signal and on the dark current. Charge transfer efficiency can basically be modeled as a random walk process in which there is a probability q that an electron makes a step to the next pixel and a probability 1-q that it resides in a pixel. For this process probability matrices can be constructed that are applied in Markov chains taking into account the "loading" by illumination and dark current. Summing up the probabilities for a complete readout results in an upper diagonal response matrix that relates the signals, that are read out at the output capacitance of the CCD, to the original charges on the CCD. Note that for charge transfer CCDs two response matrices are required: one for the transfer through the readout register and one for the transfer along the CCD columns. Symbolically, we can write

$$S_{\text{CCD}}(i,j) = \text{CTE}[S_{\text{electrons}}(i,j) + S_{\text{smear}}(i,j)] + F[S_{\text{dark}}(i,j)] \quad (7)$$

with CTE the charge transfer efficiency response function and F a complicated function describing the dark current build up and charge transfer effects on the dark current.

In summary, the signal flow on a CCD depends on the dark current build-up, the useful signal incident on the CCD, the smear signal and the charge transfer effects.

E. Read-Out Electronics

When the signal (the "parcel" of electrons) reaches the read-out electronics, the accumulated charge is converted to an analog voltage at the capacitance of the CCD. The CCD preamplifier causes a small nonlinearity in this process. The signal is further amplified by the DEM-amplifier that sets the gain, and the correlated double sampler (CDS)

$$S_{\text{Volts}}(i,j) = S_{\text{CCD}}(i,j) \cdot f_{\text{CCD}} \cdot L(S_{\text{CCD}}(i,j)) \cdot f_{\text{DEM}}(i,j) \cdot f_{\text{CDS}}. \quad (8)$$

Here, f_{CCD} is the charge-to-voltage conversion factor, the function $L(S(i,j))$ describes the nonlinearity, f_{DEM} describes the gain factor and f_{CDS} is the CDS gain. The signal is then converted from an analog video signal to a digital signal as follows. The CDS samples both the (useful) video signal and a reference level, and subtracts these samples to minimize read-out noise.

To the resulting signal a small, gain-dependent, offset voltage $V_{\text{offset}}(i,j)$ is applied to ensure a positive signal

$$S_{\text{Volts}}(i,j) = S_{\text{Volts}}(i,j) + V_{\text{offset}}(i,j). \tag{9}$$

The resulting voltage is then fed into the 12-bit analog–digital converter that converts the analog signal from (volts) to digital counts (ADC counts)

$$S_{\text{ADC}}(i,j) = S_{\text{Volts}}(i,j) \cdot f_{\text{ADC}}. \tag{10}$$

A number of individual CCD read-outs (images) will normally be co-added in the 16-bit co-addition register.

$$S_{\text{co-added}}(i,j) = \sum_{n\_\text{co-additions}} S_{\text{ADC}}(i,j). \tag{11}$$

The number of co-additions is determined by the Master Clock Period (MCP) and the exposure time (t_{exp}) that are both programmable $n\_\text{co} - \text{additions} = \text{MCP}/t_{\text{exp}}$. For each CCD one CCD pixel column is also down-linked without co-adding. These are the so-called small pixel columns. In the flight-direction their footprint is determined by the exposure time and not by the MCP (see Fig. 4).

The co-added signal and the small pixel data are the output of the read-out electronics. These signals are, after some data formatting by the electronic unit (ELU), sent to the spacecraft, via the Interface Adaptor Module, for downlink.

Equation (9) merits some additional discussion. The offset voltages V_{offset} should in principle be a constant voltage. In practice this offset shows a drift along each orbit [2]. This drift seems to correlate with the temperature of the (not-thermally stabilized) electronic unit. Studies have revealed that the offset voltage in fact contains two contributions: a gain-dependent bias from the CCD and an offset from the ELU CDS electronics that are both temperature dependent $V_{\text{offset}}(i,j) = f_{\text{DEM}}(i,j) f_{\text{CDS}} V_{\text{bias,CCD}} + V_{\text{offset,ELU}}$. In principle, the offset can be determined from the readout register after a drain dump [2]. In practice a difference was found between the offset determination from the readout register and the image area of the CCD. The empirical relation between these two is used to correct for the offset in the CCD image area using the readout register offset determination.

Another noteworthy effect is the so-called gain-overshoot. When gain switching is applied it takes the electronics a few pixel readout times to stabilize. The offset drifts during this period gradually to its new value. It is a small effect that has been modeled as an additive contribution to V_{offset} in (9).

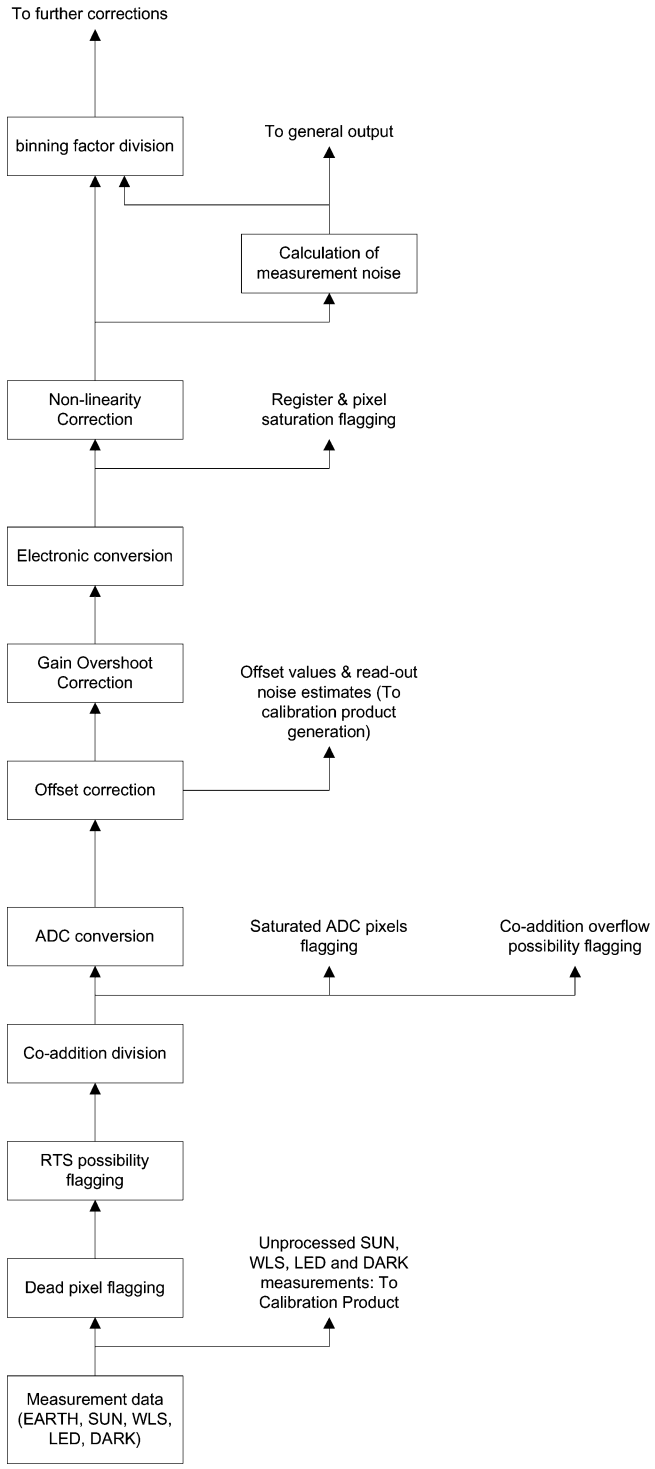

Fig. 5. Science data processing flow common to all measurement types.

V. Algorithms in the GDPS

A. Correction Algorithms

In this section, we describe the correction algorithms that are used in the GDPS. The order in which the corrections are applied, and whether they are applied, is determined by the MeasurementClass of a measurement. The science data processing flow for the different MeasurementClasses is shown in Figs. 5–10. Fig. 5 shows a generic part that applies to all MeasurementClasses.

The inversion of the forward model in the GDPS involves fifteen *correction algorithms* for radiances and one additional for irradiances. All correction algorithms use correction parameters stored in the Operational Parameters File (OPF). The offset, stray light and smear correction algorithms also use the actual signal on the CCD. The parameters stored in the OPF result from the on-ground and in-flight calibration activities as described in Section II-B. The choice to mainly use correction parameters from an OPF in stead of the actual measurements is driven by the

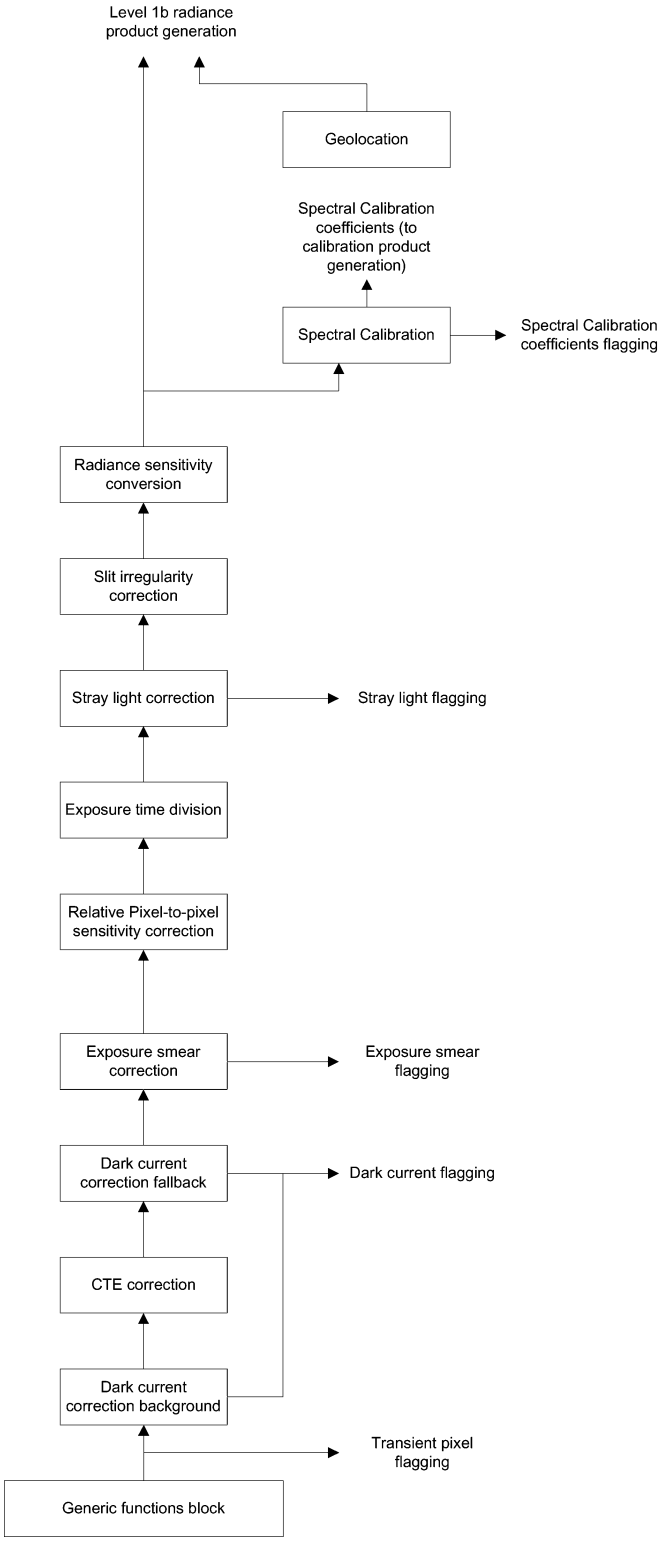

Fig. 6. Science data processing flow for EARTH measurements.

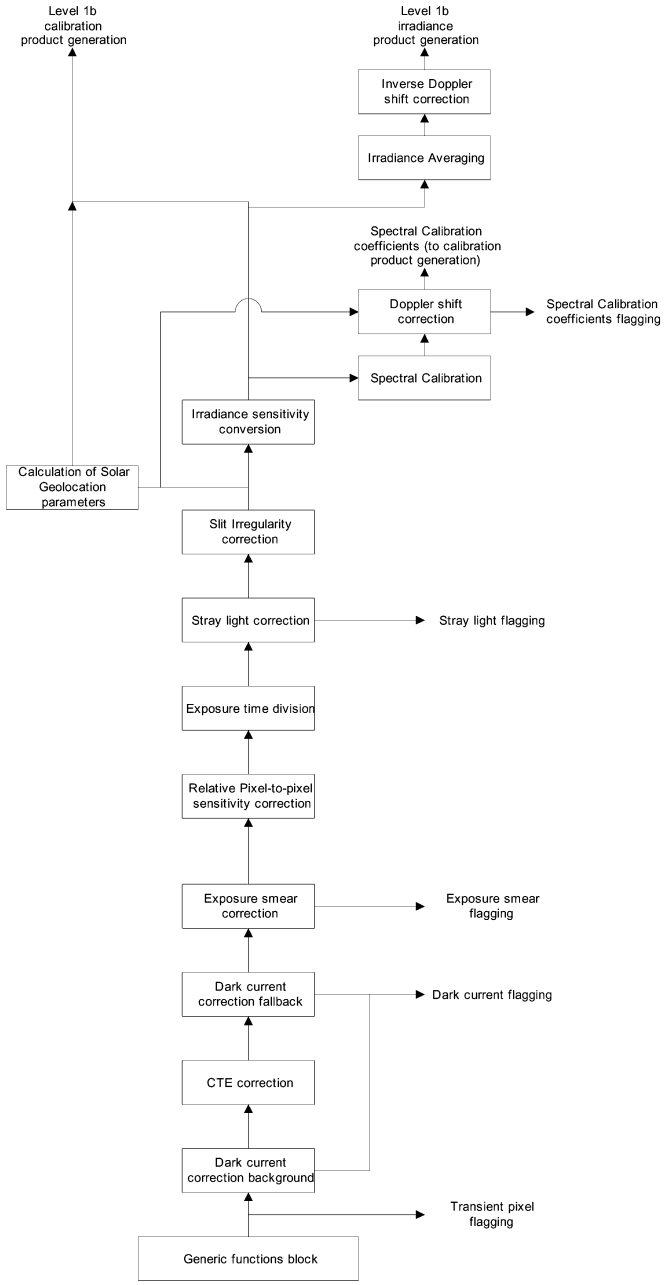

Fig. 7. Science data processing flow for SUN measurements.

fact that the parameters in the OPF are derived from numerous (calibration) measurements and, therefore, have a better precision than correction parameters based on a single measurement. However, the processor also contains a number of *flagging algorithms* that set flags in the data product when a measured parameter deviates too much from its OPF value. Next to the correction algorithms and the flagging algorithms the GDPS also contains *calculation algorithms* that are used to evaluate OPF parameters for each measurement. These calculation algorithms are not shown in the Figs. 5–10. Such an evaluation consists of applying, e.g., wavelength, binning factor, or temperature corrections to an OPF parameter. Calculation algorithms in general use OPF parameters to calculate the parameters needed in correction and flagging algorithms.

The correction steps involved are listed below with references to the applicable expressions in the forward model (Section IV). Step 17) only applies to irradiances. For the trivial and straightforward correction steps a short description is provided.

Step 1) *Co-addition division*: Division by number of co-added images (11).

Step 2) *ADC conversion*: Division by the ADC conversion factor (10).

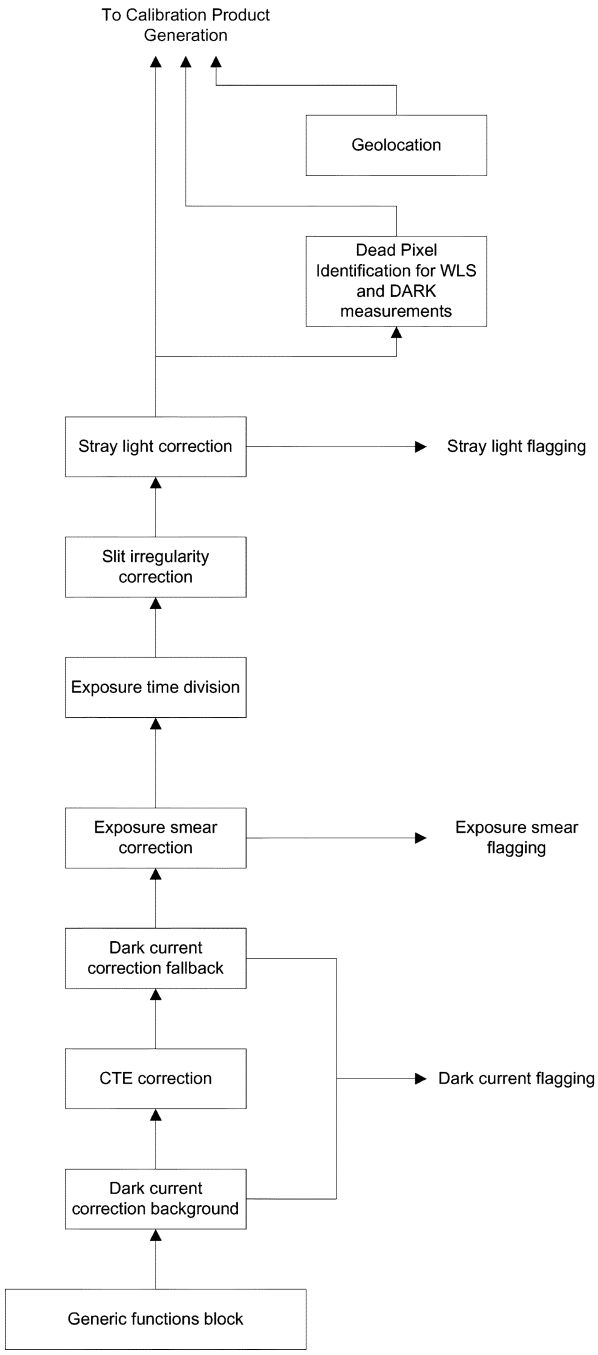

Fig. 8. Science data processing flow for WLS measurements. Dead pixel identification is currently bypassed for standard processing.

Step 3) *Offset correction*: Subtraction of the gain-dependent offset voltage (9). The GDPS determines from the readout register, after a drain dump, the average offset of all columns with a specific gain. Using OPF-based correction parameters this offset is then scaled to the offset in the image of the CCD and the resulting value is subtracted.

Step 4) *Gain overshoot correction*: For a number of pixels after a gain switch a small additional offset is subtracted (9). These values are taken from the OPF that contains values for all possible gainswitches.

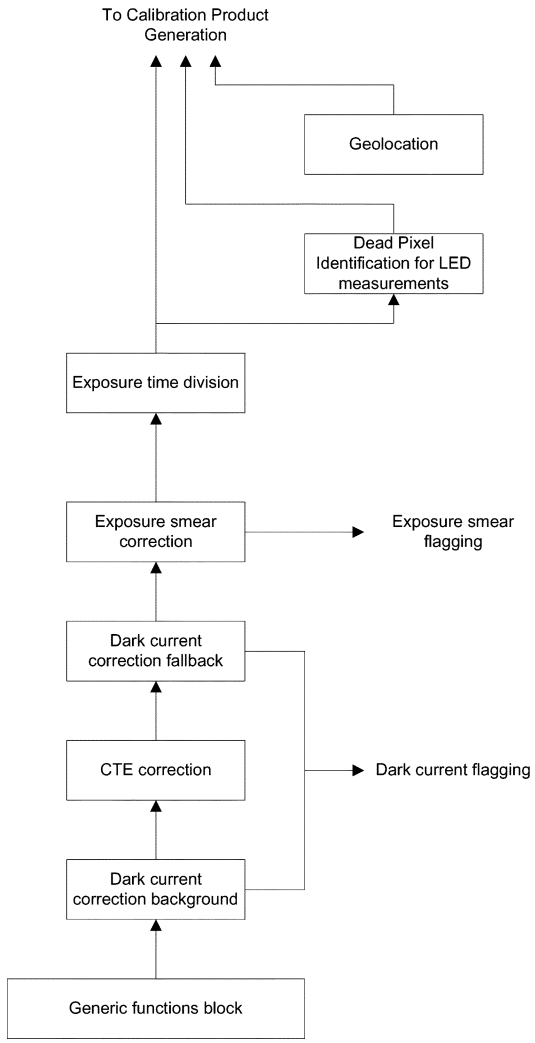

Fig. 9. Science data processing flow for LED measurements. Dead pixel identification is currently bypassed for standard processing.

Step 5) *Electronic conversion*: Division by the product $f_{\mathrm{CCD}} f_{\mathrm{DEM}} f_{\mathrm{CDS}}$ (8). This correction transforms the analog voltage to electrons on the output amplifier of the CCD and takes out the gain factor.

Step 6) *Nonlinearity correction*: This correction accounts for the nonlinearity of the CCD preamplifier (8). The correction consists of a polynomial whose coefficients are taken from the OPF.

Step 7) *Binning factor division:* Division by the binning factor used in the read-out register.

Step 8) *Dark correction background:* Subtraction of a dark current image obtained with identical CCD clocking settings as the measurement to which it is applied (7). This insures that the dark current build-up and its charge transfer effects are properly corrected for. The dark current image is taken from the OPF and is identified by the IcId and its version number. A calculation algorithm evaluates the OPF dark current image for the CCD temperature at the time of measurement. Note that the temperature dependence of the dark current is accurately known

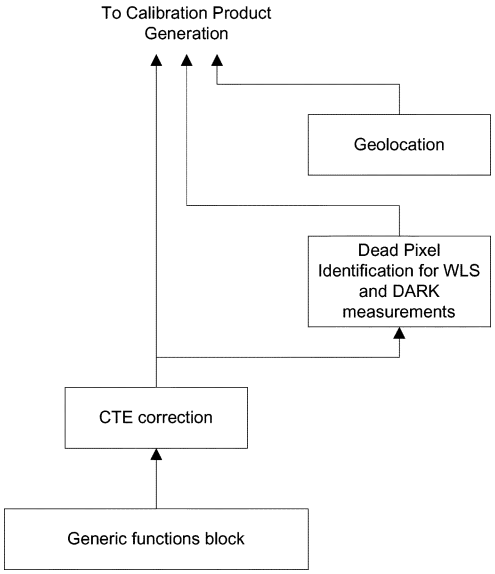

Fig. 10. Science data processing flow for DARK measurements. The CTE correction and the dead pixel identification are bypassed for standard processing.

and that the CCD temperature is very constant during nominal operations.

Because of radiation damage the dark current of individual CCD pixels may increase permanently [2]. This can only be corrected for by using the most recent background dark current images for data processing. At the time of writing the background dark images in the OPF are updated once per month. Preparations are ongoing to be able to provide an OPF for each orbit that contains the actual dark measurements of that orbit. This will be used for reprocessing campaigns.

Step 9) *Charge transfer efficiency (CTE) correction:* First, all CCD rows, each considered as a vector, are multiplied by the inverse CTE response matrix for horizontal charge transfer in the read-out register. Then all CCD columns, each again stored as a vector, are multiplied by the inverse CTE response matrix for vertical charge transfer. In case of binning, the response matrix for that pixel, in a collection of binned pixels that is closest to the readout register is used. In principle the response matrices are upper-diagonal but, because the CTE of OMI is currently very good, only a band diagonal matrix is used and other off-diagonal elements are taken zero. When the background dark correction has been applied the term $F\left[S_{\mathrm{dark}}(i,j)\right]$ in (7) has already been corrected for and the CTE correction algorithm only acts on the useful signal and the smear signal. In the case that the OPF does not contain a background dark image for a specific instrument configuration the CTE correction works on the combined useful, smear and dark signal. Currently the charge transfer over the OMI CCDs is so good that this algorithm is effectively not applied.

Step 10) *Dark correction fallback:* In case a background dark current image for a specific instrument configuration is not available in the OPF a synthetic dark image is constructed by the GDPS. The OPF contains pixel-based dark current maps. Based on the CCD clocking sequence during the measurement the resulting dark current in each pixel is calculated. It contains contributions from the exposure, the frame transfers, and the CCD readout. Also, a temperature correction is applied to account for the CCD temperature at the time of the measurement.

Step 11) *Exposure smear correction:* Subtraction of smear contribution. In the OPF the users can set a parameter to preselect the correction algorithm that will be applied. One algorithm subtracts an estimate of the integrated signal along a CCD column multiplied by the ratio of the frame transfer time (4.32 ms) and the exposure time (nominally 0.4 s). This algorithm is exact in case of constant illumination (in time). Because during readout of the CCD various pixel rows are skipped there is no information available about the illumination levels at those pixels. The algorithm determines the average signal levels inside and outside the image area of the CCD (using, e.g., information from the stray light rows) and then calculates the smear contribution from the known number of CCD rows inside and outside the image area.

The second algorithm is based on a linear interpolation over the CCD (in the swath direction) between the smear signal in the masked upper and lower dark rows. This algorithm corrects to some extent for time variations in the scene but is more sensitive to noise. The first method is the baseline for standard processing.

Step 12) *PRNU correction:* Divides the CCD image by a PRNU map (6). In this way the pixel-to-pixel variations in quantum efficiency at a specific wavelength are accounted for. For binned images the average PRNU values of the binned pixels are used in the algorithm. This corresponds to the approximation that each of the binned pixels has received an equal number of photons.

Step 13) *Exposure time division:* Division by the exposure time used during the measurement.

Step 14) *Stray light correction:* Subtraction of spectral stray light (3). Reference [2] provides a detailed discussion of the stray light features in OMI. Currently the stray light correction algorithm is fairly straightforward. In the OPF a number of wavelength ranges is given that define so-called source and target regions. For each source region the average signal is calculate using the information over the complete swath. This signal, multiplied by a transfer-factor from the OPF, is subtracted from all pixels in a target region. The transfer-factor is a polynomial that distributes the stray light over the source region. There is also

TABLE II
PIXEL QUALITY FLAGS

Pixel Quality Flag/Description
MISSING flag This flag indicates that information for the pixel was not available in the level 0 input data. The contents of this pixel should not be used for further science processing.
BAD_PIXEL flag This flag indicates that the pixel is either a dead pixel or has too high pixel filling, causing saturation of the A/D converter. Dead and bad pixels are specified by means of a list in the OPF. Binned pixels correspond to multiple pixels on the CCD. If at least one of these CCD pixels is specified as bad or dead in the OPF, this flag is raised for the measurement pixel. When this flag is raised, the information for this pixel is unreliable and should not be used.
PROCESSING_ERROR flag This flag indicates that an unexpected error occurred in one of the algorithms. As a result, the information for this pixel is unreliable and should not be used.
TRANSIENT_PIXEL_WARNING flag This flag indicates that the pixel has been identified as transient. This flag indicates particle hits on the detectors.
RTS_PIXEL_WARNING flag This flag indicates that the pixel may be subject to Random Telegraph Signal (RTS) behaviour [2]. RTS pixels are specified by means of a list in the OPF. Binned pixels correspond to multiple pixels on the CCD. If at least one of these CCD pixels is specified as RTS pixel in the OPF, this flag is raised for the measurement pixel.
SATURATION_POSSIBILITY_WARNING flag This flag indicates that the pixel has too high pixel filling, causing saturation in the CCD detector. This can either be because the average unbinned contents exceed the pixel full well or the binned contents exceed the register full well. The limit for saturation is specified in the OPF, and is set to a value where pixels are flagged when they reach the limit for the ellipsoid effect. The flag is also set when there are indications that an amplifier in the signal chain is likely saturated.
NOISE_CALCULATION_WARNING flag The noise values in the GDPS are calculated as the combination of shot-noise and read-out noise. The shot-noise is equal to the square-root of the signal. When the signal drops below 0, which is possible when for example the noise is larger than the signal, the shot-noise cannot be calculated and noise values will only be based on the read-out noise. In that case, the noise calculation warning flag is raised.
DARK_CURRENT_WARNING flag The dark current that is subtracted from each measurement is compared to a region on the CCD that only contains dark current. The average and standard deviation of this region are calculated from the measured image and compared to the average of the dark current correction coefficients for the same region. When the averages differ more than is expected from the standard deviation, this warning flag will be raised. The number of times the standard deviation that the averages are allowed to differ is specified in the OPF.
OFFSET_WARNING flag In the offset values of the electronics and the CCD drifts are observed. To compensate for this drift, a dynamic offset value is calculated from the measurement itself. These dynamic offset values are compared to expected values. When the deviation between the calculated and dynamic value is more than expected, this flag will be raised for all pixels that have been corrected with the dynamic value. The limits for flagging are specified in the OPF.

Pixel Quality Flag/Description
EXPOSURE_SMEAR_WARNING flag The GDPS will calculate the correction coefficients for exposure smear from the measurements. For each column in the measurement the sum of the exposure smear correction coefficients is compared to the sum of the pixels in the measurement after smear correction. When the (sum of the) exposure smear exceeds the (sum of the) signal more than an expected fraction, this flag is raised for all pixels in that column. The limit for flagging is specified in the OPF.
STRAY_LIGHT_WARNING flag The stray light warning flag indicates a potential under- or overcorrection in the stray light correction algorithm. There are several conditions for which the flag is raised: 1) The stray light correction coefficients consist of several components, including stray light that is measured through the stray light areas on the CCD and several components that are calculated from the signal levels in specific wavelength bands. When one or more of the components for the stray light correction coefficient for a pixel cannot be calculated, the stray light warning flag will be raised. 2) When the calculated stray light contribution for a specific pixel exceeds the total signal for that pixel, the stray light warning flag will be raised. 3) The sum of the stray light correction coefficients are compared to the sum of the total signal for regions that are expected to have a fairly constant signal to stray light ratio. When the sum of the stray light exceeds an expected fraction of the sum of the signal, the stray light warning flag is raised for all the pixels in the region. The expected fraction is specified per region, together with the region extents, in the OPF.
NON_LIN_WARNING flag This flag indicates that the signal for the pixel is in the non-linear range of the CCD pre-amplifier. The GDPS will use an algorithm to correct for the non-linearity effects, but some residuals may exist. The non-linear range is specified in the OPF.
OPF_OFFSET_WARNING flag The GDPS will calculate a dynamic offset for offset correction in order to compensate for drifts. When a dynamic offset value cannot be determined, an offset value from the OPF will be used as fallback. In that case, this flag is raised for all pixels for which the OPF offset value was used to indicate that there may be inaccuracies in the offset correction.
DEAD_PIXEL_IDENTIFICATION flag Currently not used. Dead pixels are identified in off-line analyses.
DEAD_PIXEL_IDENTIFICATION_ERROR flag Currently not used.
WAVELENGTH_ASSIGNMENT_WARNING flag The GDPS applies a correction for small wavelength shifts that result from inhomogeneous slit illumination to the wavelength assignment polynomial coefficients. This correction is based on the data in the small pixel columns. In case the correction coefficients cannot be calculated, for example when the small pixel columns are not available or contain unreliable values, this flag will be raised for all affected pixels. The Level 1b data can still be used, but there may be a slight inaccuracy in the wavelength assignment.

the possibility to subtract the signal in the stray light rows above and below a target region from the pixels in the target region.

Step 15) *Slit irregularity correction:* Division by a function that describes the slit irregularity [ρ in (6)]. For binned measurements the function is first binned before applying the correction.

Step 16) *Radiance Sensitivity (EARTH) and Irradiance Sensitivity (SUN) correction:* Multiplications with the radiance sensitivity function or the irradiance sensitivity function [$\Re$ in (6)]. These functions are stored for each pixel in the OPF as a function of wavelength and CCD row. The algorithm interpolates these functions to the actual wavelength of each pixel during the measurement. This accounts for variations of the wavelengths due to temperature variations of the optical bench (telescope and spectrograph) along the orbit. Also,

the functions are binned in case of binned measurements.

For the irradiance sensitivity correction an additional step is required because the irradiance calibration depends on the incident angles of the solar signal on a diffuser. This function is stored in the OPF for each diffuser in the form of the coefficients of a multi-dimensional polynomial that depends on the solar azimuth angle, the solar elevation angle, CCD row and wavelength [2]. The algorithm evaluates the polynomial for each measurement and the signal is divided by the result.

Step 17) *Irradiance averaging:* Each solar observation consists of multiple measurements at different elevation angles. The algorithm averages the individual measurements to improve the signal-to-noise ratio and to average out variations caused by diffuser features that vary with the solar elevation angle. Pixels that are identified as transients are excluded from this average. The algorithm also permits calculation of a running average over the CCD rows to further minimize the effect of diffuser features. The number of CCD rows involved in the average is a tuneable parameter but cannot be too large because of the spectral smile. A too large value would effectively result in a widening of the slit function.

The noise associated with the signal is calculated in a straightforward way. The signal (in electrons) consists of a photon-induced signal and a dark signal contribution. Both the photon-induced signal and the dark current shot noise are assumed to be Poisson noise. To these Poisson noise contributions the small contribution by the readout noise is added. The latter is obtained from the variance of the signal in the readout register after a drain dump. The noise is calculated after the nonlinearity correction and then propagated through the remaining correction steps. Because an increasing number of CCD pixels exhibit random telegraph signals (RTS) this noise model needs to be revised. RTS is the effect that pixels that suffer from radiation damage exhibit dark current levels that vary in time [2]. For pixels showing small amplitude RTS behavior it is possible to interpret this behavior as an additional noise contribution. In the near future this will be included in the GDPS.

For most pixel-dependent parameters (dark maps, PRNU, radiance conversion functions, wavelength polynomial parameters), the OPF contains values for unbinned measurements. This is useful because it allows, via averaging, the OPF entries to be applied to all measurement types regardless different binning factors. Also new measurement types can easily be introduced without introducing large changes in the GDPS and the OPF. It means that the GDPS computes for each measurement row the corresponding first- and last CCD row and averages the parameters from these rows and the rows in between.

There is, however, a limitation coupled to this method, which is clear if we write out the equations for a general correction with n rows binnned. The measurement forward model step shows up as follows:

$$S_{\text{measured}} = \frac{1}{n} \cdot \sum_{i=1}^{n} \alpha_i \cdot S_i.$$

But, after correction, we do not exactly retrieve the average of S_i

$$S_{\text{corrected}} = S_{\text{measured}} \Big/ \frac{1}{n} \cdot \sum_{i=1}^{n} \alpha_i \neq \frac{1}{n} \cdot \sum_{i=1}^{n} \cdot S_i \, .$$

For smoothly varying calibration parameters ($\alpha_i \approx$ constant) the discrepancy disappears and this is the case for the majority of the cases. A problem exists for the radiance and irradiance correction at the most extreme viewing angles. The radiometric sensitivity of OMI drops so rapidly at these rows that the approximation fails. Level 2 products do not to seem to suffer from this effect but more detailed studies and product validation are required to come to a final assessment.

B. Spectral Calibration

The procedure for spectral calibration is based on the fact that the spectral calibration of OMI changes only slightly as a function of the temperature of the optical bench (OPB). Furthermore, OMI provides a very stable thermal environment with a high repeatability of the OPB temperature along the orbit. Therefore, it has been decided to parameterise the wavelength calibration as a function of OPB temperature and CCD column number. The OPB temperature is a weighted average of the four temperatures that are measured by four thermistors at various locations on the OPB.

The OPF contains wavelength polynomial coefficients for all image rows for a given reference temperature of the OPB. The OPF also contains polynomial coefficients to evaluate the wavelength polynomial coefficients at different OPB temperatures. The temperature of the OPB at the time of a measurement is used to calculate corrected wavelength polynomial coefficients for each image row, that is, for each (ir)radiance spectrum. These corrected wavelength polynomial coefficients are provided in the Level 1b radiance and irradiance products. The reason for providing wavelength polynomial coefficients in the Level 1b data products, in stead of providing actual wavelengths, is that it considerably reduces the size of a data product.

The aforementioned steps are referred to as wavelength assignment. Based on in-flight results it turned out that for the wavelength assignment for radiance measurements an additional step was needed. Inhomogeneous scenes (mainly because of the presence of clouds) result in an inhomogeneous illumination of the spectrograph entrance slit. As a consequence the effective slit function is weighted with the illumination pattern resulting in small wavelength shifts. It turns out that an empirical relation exists between the measured variations in the small pixel signals and the observed wavelength shifts. This empirical relation is used in the GDPS to correct for these variations.

Next to the wavelength assignment the GDPS also performs a wavelength calibration for each measured irradiance spectrum

and each nadir radiance spectrum. The result of this calibration, in terms of wavelength polynomial coefficients, is stored, together with the OPB temperature and the OPB thermistor readings, in the Level 1b Calibration product. This product is used in off-line analyses to derive and monitor the wavelength and OPB-temperature polynomial coefficients contained in the OPF. The rationale for this approach is that the spectral calibration, resulting from many spectral fits, is anticipated to be more accurate and stable than the spectral calibration obtained from an individual measurement.

The spectral calibration that is performed on each spectrum is based on a fit of the Fraunhofer structures in optimized spectral windows in the UV-1, UV-2, and VIS channel. Typically 6 to 21 windows are used in a channel. The central wavelengths of these windows are determined by the fits. Then a polynomial fit is performed over each (sub)channel and the resulting polynomial coefficients are written to the Level 1b Calibration product (evaluation of a polynomial gives wavelength as function of CCD pixel column number).

Each (nonlinear) fit is based on minimizing, in chi-square sense, the differences between a high-resolution solar spectrum, convoluted with the OMI slit function and therefore at OMI resolution, and the measured spectrum in a window. For radiance measurements it is possible to include an ozone cross section and a Ring contribution in the fit (both at OMI resolution). Also, it is possible to choose between a direct fit of the measured spectrum or the logarithm of this spectrum.

Of paramount importance for the above outlined approach is that during the on-ground calibration period the slit function of OMI has been measured on pixel level. The combination of an accurately known slit function, together with a high-resolution solar spectrum, provides the required spectral knowledge.

The solar spectrum and the Ring spectrum (both at OMI resolution) that are used for spectral calibration are stored in the OPF at laboratory wavelengths. Because measured irradiance spectra are Doppler shifted these are first Inverse Doppler shifted, then the spectral fit is performed and finally the result is again Doppler shifted before being written in the output product.

C. Geolocation Calibration

Based on the elevation and azimuth angles for each pixel line of sight, the time of measurement and the spacecraft ephemeris attitude the SDP toolkit [5] is used to determine the geolocation of the center of each groundpixel. The spacecraft attitude data serves as an external input to geolocation calculation. In the flight direction the time stamp at the middle of all co-added exposures is used. In the swath direction the lines of sight of the pixels involved, taken from the OPF, are averaged over a range of CCD columns. This makes the geolocation assignment independent of wavelength for each subchannel. Note that the lines of sight are given with respect to the spacecraft alignment cube.

In addition to geolocation the Level 1b radiance product also contains other relevant information such as solar zenith angles, terrain height, snow-ice and land-water information, spacecraft manoeuvre flagging, South Atlantic Anomaly flagging, solar eclipse possibility flagging, and sun glint possibility flagging.

TABLE III
GROUND PIXEL QUALITY FLAGS

Ground Pixel Quality Flag/Description
Land/Water flags Land / Water flags are included for all ground pixels in the Level 1b radiance output products based on the 90 arcsec Digital Elevation Model (DEM) of the SDP Toolkit.
Sun Glint Possibility flag The Sun Glint Possibility flag is raised for ground pixels that may be subject of sun glint, i.e. direct reflection of sunlight at the earth's surface. Sun Glint will be calculated based on the solar zenith and azimuth angles from the ground pixel location and the spacecraft zenith and azimuth angles from the ground pixel location. The Sun Glint Possibility flag is raised in case the following equation is fulfilled: $\arccos\left[\begin{array}{l}\cos(\theta_1).\cos(\theta_2)- \\ \sin(\theta_1).\sin(\theta_2).\cos(\varphi_1-\varphi_2)\end{array}\right] \le sun\_glint\_possibility\_threshold$ Where: ϕ_1= is the sun azimuth angle from the ground pixel location ϕ_2= is the spacecraft azimuth angle from the ground pixel location θ_1= is the sun zenith angle from the ground pixel location θ_2= is the spacecraft zenith angle from the ground pixel location The sun glint possibility threshold is specified in the OPF.
Solar Eclipse possibility flag This flag indicates that a ground pixel may be affected by a solar eclipse. For each of the solar eclipses during the mission the OPF contains a rectangular latitude / longitude bounding box that specifies the affected region and a start time and stop time of the solar eclipse. When a ground pixel meets these specifications, the Solar Eclipse possibility flag is raised.
Geolocation Error flag This flag indicates that an error occurred during the ground pixel geolocation. One or more of the ground pixel geolocation parameters, such as latitude and longitude, but also fields like terrain height and land / water flags could be affected. The ground pixel geolocation fields should not be trusted.
Snow/Ice flags Snow / Ice flags are included for all ground pixels in the Level 1b radiance output products based on the Near Real-Time SSM/I EASE-Grid Daily Global Ice Concentration and Snow Extent (NISE) data product. Since NISE contains undefined or unreliable data at several locations, especially around coast lines, a nearest neighbour interpolation algorithm is used for finding snow / ice flags for such pixels.
NISE nearest neighbour filling flag This flag is raised by the GDPS to indicate that the NISE data product contained an undefined or unreliable snow / ice cover value for the ground pixel and therefore a nearest neighbour interpolation algorithm was used to find a proper value. The result of the nearest neighbour algorithm is stored in the snow / ice flags.
Geolocation warning flag This flag indicates a problem with the Solar or Spacecraft zenith or azimuth angle from the ground pixel location. Either one or more of the azimuth angles could not be calculated because the vector was below the horizon (this can occur for measurements near the eclipse), or refraction was not taken into account in the calculation of one or more of these angles (this can occur for extreme zenith angles).

VI. FLAGGING AND METADATA

The OMI Level 1b data products contain, of course, essential physical parameters like radiances or irradiances, wavelengths and geolocation information [6]. This is the basic information needed for higher level product generation. This information is, however, almost useless without any information about potential issues that affect the quality of the data. For that purpose an extensive flagging is applied in the GDPS. At a higher level statistics can be collected about the flagging properties in a data product file. These serve to support the quality assessment (QA)

TABLE IV
MEASUREMENT QUALITY FLAGS

Measurement Quality Flag/Description
Instrument Test Mode flag This flag indicates that a test mode of the instrument electronics was used. Data / measurements that have this flag raised should be discarded for further science data processing.
Alternative Engineering Data flag This flag indicates that, as a result of data gaps or errors in the Level 0 data, the engineering data for the measurement could not be found and / or used by the GDPS. Since OMI is often operated with the same measurement settings for a long series of consecutive measurements, the GDPS has tried to process the science data with the first available engineering data before or after the measurement. When this 'alternative' engineering data does not match the measurement, as a result, pixels may have been extracted at erroneous locations in the measurement, wrong gain corrections may have been used, etcetera. Great caution should be taken when using this data for further science processing. It is recommended to discard this data.
Alternating Sequencing Readout flag This flag indicates that the alternating sequencing mode of the instrument is used, where exposure and read-out are alternated. This is different from nominal mode where constantly exposure is taking place and during one read-out a new exposure is taking place for the next read-out. Alternating read-out mode is required for very short exposure times, but results in gaps between the exposures. Alternating sequencing mode is currently not foreseen for nominal operations.
Co-adder Error flag This flag indicates that an error occurred in the co-addition function of the instrument electronics. Data / measurements that have this flag raised should be evaluated before further science data processing.
Invalid Co-addition Period flag This flag indicates that the co-addition period / master clock period is not a multiple of the exposure time and / or read-out time. As a result of this, the last exposure is shortened or extended. The GDPS compensates for this in the algorithms, but the instrument should be commanded to avoid this situation. Therefore, when this flag is raised, it may indicate possible problems in instrument commanding and as such serves as a warning for further science data processing.
Co-addition Overflow Possibility flag This flag indicates that more than 16 co-additions were used in the measurement. As such, overflow may occur for the co-added pixels.
Measurement Combination flag This flag indicates that level 0 data from multiple co-addition periods / master clock periods was combined into a single measurement. This is the case for so-called unbinned measurements and long exposure measurements that are read-out in multiple master clock periods. This flags serves as a notification; it is not a warning or error flag to indicate bad data or potential problems.

Measurement Quality Flag/Description
Rebinning flag This flag indicates for measurements in the Level 1b global radiance products that the data was acquired using a zoom mode but was resampled to the nominal resolution for inclusion in the Level 1b global data product. This flags serves as a notification; it is not a warning or error flag to indicate bad data or potential problems.
Dark Current Correction Processing Option flag The GDPS supports two different algorithms for dark current correction. This flag indicates which of the two algorithms was used.
Detector Smear Calculation Processing Option flag The GDPS supports two different algorithms for exposure smear correction. This flag indicates which of the two algorithms was used.
SAA Possibility flag This flag indicates that the (quality of the) data may be affected by the South Atlantic Anomaly. The SAA Possibility flag is raised when the spacecraft sub-satellite point lies within a rectangular latitude / longitude bounding box that is specified in the OPF.
Spacecraft Manoeuvre flag This flag indicates that the (quality of the) data may be affected by a Spacecraft Manoeuvre. The Spacecraft Manoeuvre flag is raised when the distance on the earth surface (based on a spherical approximation) between the spacecraft sub-satellite point and the ground pixel associated with the nominal nadir point vector exceeds a threshold that is specified in the OPF.
Geolocation Error flag This flag indicates that an error occurred in the geolocation routines. None of the geolocation fields for this measurement should be trusted.
D/S Gain Offset warning flag The GDPS will calculate a dynamic offset for offset correction in order to compensate for drifts. When a dynamic offset value cannot be determined, an offset value from the OPF will be used as fallback. The dynamic offset value is calculated from the Read-out Register. Since the offset is gain dependent and the gain for the Dark Current and Stray Light areas on the detector can be different from all the gains used in the Read-out Register, it can occur regularly that it is not possible to calculate the dynamic offset value for the Dark Current and Stray Light areas and the OPF fallback value will be used for the offset correction in these areas. In that case, this flag will be raised. Note that there is also a Pixel Quality Flag to flag the affected pixels.

effort. Both flagging and QA statistics in OMI Level 1b data products are described in this section.

A. Level 1b Data Product Flags

The Level 1b data products include a series of flags that provide information on the quality of the data. The purpose of these flags is as follows.

- Inform the users of the data about the reliability of the information. This is especially important when the data is used for Level 2 processing.
- Provide the (in-flight) calibration scientists with information to assess on high-level the performance of the instrument and/or the GDPS.
- Provide information for the purpose of quality assessment (QA).

The flags are stored in the Level 1b products at several levels.

- Pixel Quality Flags, which provide information for a single (binned) pixel in the measurement (Table II).
- Ground Pixel Quality Flags, which provide information for a groundpixel; only radiance measurements are associated with groundpixels (Table III).
- Measurement Quality Flags, which provide information that is applicable to all the data from one of the (sub)channels of a measurement (Table IV)
- Spectral Calibration Flags, which provide information on the data that results from the spectral calibration algorithm. These flags appear only in the Level 1b calibration product (OML1BCAL) and are not further discussed here.

Tables II–IV list the flags that appear in the Level 1b radiance and irradiance products and describe their purpose.

TABLE V
QUALITY ASSESSMENT PARAMETERS

Attribute (Level)/Description
AutomaticQualityFlag (Metadata) This attribute is assigned a value based on the percentage in the attributes QAStatPctPixBad, QAStatPctPixProcessingError, QAStatPctGeolocationError, and QAStatPctMeasError. The flag is set to "Failed" if any of the values of these attributes is greater than the value of the PCF parameter "`AutQualFlagFailedThreshold`" The flag is set to "Suspect" if all of the values of these attributes are greater than the value of the PCF parameter "`AutQualFlagSuspectThreshold`" but less than or equal to the value of the PCF parameter "`AutQualFlagFailedThreshold`" The flag is set to "Passed" is all of the values of these attributes are less than the value of the PCF parameter "`AutQualFlagSuspectThreshold`"
QAStatPctMeasError (Measurement) Percentage of measurements with at least one of the following error flags set: the alternative engineering data flag, the co-adder error flag and the geolocation error flag
QAStatPctMeasWarning (Measurement) Percentage of measurements for which at least one of the MeasurementQualityFlags was set as a warning, excluding the alternative engineering data flag, the co-adder error flag and the geolocation error flag in the count
QAStatPctGeolocationError (Ground pixel) Percentage of ground pixels for which the geolocation determination resulted in the GroundPixelQualityFlag for geolocation error being set
QAPercentMissingData (Pixel) Percent of data for which the PixelQualityFlags has the MISSING FLAG raised.
QAStatPctPixBad (Pixel) Percentage of image pixels for which the PixelQualityFlags has the BAD_PIXEL flag set.
QAStatPctPixProcessingError (Pixel) Percentage of image pixels for which the PixelQualityFlags has the PROCESSING_ERROR flag set
QAStatPctPixWarning (Pixel) Percentage of image pixels for which the PixelQualityFlags has at least one of the following PixelQualityFlags set: TRANSIENT_PIXEL_WARNING, RTS_PIXEL_WARNING, SATURATION_POSSIBILITY_WARNING, NOISE_CALCULATION_WARNING, DARK_CURRENT_WARNING, OFFSET_WARNING, EXPOSURE_SMEAR_WARNING, STRAY_LIGHT_WARNING, NON_LIN_WARNING, and OPF_OFFSET_WARNING

TABLE VI
INSTRUMENT CONFIGURATION VERSUS ORBIT TYPE

	Global orbit scenarios							Spatial zoom-in orbit scenarios	
	N1	D	W1	W2	W3	M2	M3	N2	M1
Earth	2/7 [1]	2/7	2/7	2/7	2/7	2/7	141+142	44/49 [1]	44/49
	1	1	1	1	1	1	(25x) [2]	43	43
	0	0	0	0	0	0		42	42
	1	1	1	1	1	1		43	43
	2	2	2	2	2	2		44	44
Solar		8	14	18		30			50
		9	15	19		31			51
	S/C enters eclipse								
Calibraion		12	16	20	26	32			175 [3]
		13	17	21	27	33			176 [4]
		141			28	34			
		142			29	35			
	3	10		22	22			45	52
	4	11		23	23			46	53
	5	103 (9x)		24	24			47	54
	6			25	25			48	55
	S/C midnight								
	3			22	22	36		45	52
	4			23	23	37		46	53
	5			24	24	38		47	54
	6			25	25	39		48	55
	S/C exit eclipse								

Notes:
1) IC = 7 and 49 only during the ozone hole season above the Antarctic.
2) IC = 141 + 142 are dark measurements, repeated 25 times to completely cover the M3 orbit.
3) This is a whole series of LED linearity dark measurements with IC = 175, 147, 151, 155, 159, 163, 167, 171, 169, 165, 161, 157, 153, 149, 177, 173.
4) This is a whole series of LED linearity measurements with IC = 176, 148, 152, 156, 160, 164, 168, 172, 170, 166, 162, 158, 154, 150, 178, 174.

B. Metadata QA Statistics

For each of the output products, the GDPS produces metadata. Metadata describes the quality and characteristics of the data products, and is written using the SDP toolkit library. The contents and format of the metadata attributes are described in [6]. The quality of the data product is described by the set of so-called QA statistics parameters. Table V describes those attributes and what they tell about the quality of the product.

The generic approach for the population of the QA statistics percentage attributes is as follows.

- Each calibration product attribute is calculated for UV and VIS measurements separately.
- Each radiance and irradiance product attribute is calculated for UV1, UV2, and VIS measurements separately.

This approach is used for the following attributes:

- Measurement-based statistics:
  —QAStatPctMeasError
  —QAStatPctMeasWarning
- Groundpixel-based statistics:
  —QAStatPctGeolocationError
- Pixel-based statistics:
  —QAStatPctPixBad
  —QAStatPctPixProcessingError
  —QAStatPctPixWarning

As an example, for the attribute QAStatPctPixBad, this means that for the radiance and irradiance products, the following attributes are incorporated in the GDPS code:

- QAStatPctPixBadUV1;
- QAStatPctPixBadUV2;
- QAStatPctPixBadVIS.

And for the calibration product the following attributes are incorporated in the GDPS code:

- QAStatPctPixBadUV;
- QAStatPctPixBadVIS.

The calculation of the QA statistics on pixel flags and measurement flags is done separately for UV1, UV2, and VIS. This means that for the UV channel, a difference is made between the

TABLE VII
INSTRUMENT CONFIGURATION VERSUS MEASUREMENTCLASS AND ORBIT TYPE

ICID	ICID descriptor	ELU	Msmnt Class	Orbit Type
0	global tropical	1	EARTH	N1,D, M2,W1, W2,W3
1	global midlatitude	2	EARTH	
2	global arctic	3	EARTH	
3	global tropical dark, no FMM	1	DARK	N1
4	global midlatitude dark, no FMM	2	DARK	N1
5	global arctic dark, no FMM	3	DARK	N1
6	global ozone hole dark, no FMM	4	DARK	N1
7	global ozone hole	4	EARTH	*N1,D, M2,W1,W 2,W3*
8	solar cal, volume diffusor, BF8	28	SUN	D
9	solar cal dark, volume diffusor, BF8	28	DARK	D
10	LED dark, unbinned	22	DARK	D
11	LED, unbinned	22	LED	D
12	long dark unbinned, short duration	14	DARK	D
13	long dark unbinned, long duration	15	DARK	D
14	solar cal, volume diffusor, BF1	26	SUN	W1
15	solar cal dark, volume diffusor, BF1	26	DARK	W1
16	long dark 4 gains	16	DARK	W1
17	long dark 1 gain	17	DARK	W1
18	solar cal, regular diffusor, BF8	24	SUN	W2
19	solar cal dark, regular diffusor, BF8	24	DARK	W2
20	WLS PRNU dark	23	DARK	W2
21	WLS PRNU	23	WLS	W2
22	global tropical dark, FMM	1	DARK	W2,W3
23	global midlatitude dark, FMM	2	DARK	W2,W3
24	global arctic dark, FMM	3	DARK	W2,W3
25	global ozone hole dark, FMM	4	DARK	W2,W3
26	LED stability dark	31	DARK	W3
27	LED stability	31	LED	W3
28	WLS stability dark BF8	30	DARK	W3
29	WLS stability BF8	30	WLS	W3
30	solar cal, backup diffusor, BF8	25	SUN	M2
31	solar cal dark, backup diffusor, BF8	25	DARK	M2
32	LED dark, 4 gains used	18	DARK	M2
33	LED dark, 1 gain used	19	DARK	M2
34	LED, 4 gains used	18	LED	M2
35	LED, 1 gain used	19	LED	M2
36	WLS dark, 4 gains used	20	DARK	M2
37	WLS dark, 1 gain used	21	DARK	M2
38	WLS, 4 gains used	20	WLS	M2
39	WLS, 1 gain used	21	WLS	M2
40	WLS linearity #1 dark	29	DARK	L
41	WLS linearity #1	29	WLS	L
42	spatial tropical	5	EARTH	N2,M1
43	spatial midlatitude	6	EARTH	N2,M1
44	spatial arctic	7	EARTH	N2,M1
45	spatial tropical dark, no FMM	5	DARK	N2
46	spatial midlatitude dark, no FMM	6	DARK	N2
47	spatial arctic dark, no FMM	7	DARK	N2
48	spatial ozone hole dark, no FMM	8	DARK	N2
49	spatial ozone hole	8	EARTH	*N2,M1*
50	solar cal, volume diffusor, BF4 (spatial)	27	SUN	M1
51	solar cal dark, volume diffusor, BF4	27	DARK	M1
52	spatial tropical dark, FMM	5	DARK	M1
53	spatial midlatitude dark, FMM	6	DARK	M1
54	spatial arctic dark, FMM	7	DARK	M1
55	spatial ozone hole dark, FMM	8	DARK	M1
56	spectral tropical	9	EARTH	Z
57	spectral midlatitude	10	EARTH	Z
58	spectral arctic	11	EARTH	Z
59	spectral tropical dark, no FMM	9	DARK	Z
60	spectral midlatitude dark, no FMM	10	DARK	Z
61	spectral arctic dark, no FMM	11	DARK	Z
62	solar cal, volume diffusor, BF4 (spectral)	32	SUN	Z
63	solar cal dark, volume diffusor, BF4	32	DARK	Z
64	spectral tropical dark, FMM	9	DARK	Z
65	spectral midlatitude dark, FMM	10	DARK	Z
66	spectral arctic dark, FMM	11	DARK	Z
67	SLS nadir Port performance	37	ONGROUND	G
68	LEO solar cal, regular diffusor, BF4	33	SUN	L
69	LEO solar cal dark, regular diffusor, BF4	33	DARK	L
70	LEO solar cal, regular diffusor, BF1	34	SUN	L
71	LEO solar cal dark, regular diffusor, BF1	34	DARK	L
72	LEO solar cal, backup diffusor, BF4	35	SUN	L
73	LEO solar cal dark, backup diffusor, BF4	35	DARK	L
74	LEO solar cal, backup diffusor, BF1	36	SUN	L
75	LEO solar cal dark, backup diffusor, BF1	36	DARK	L
76	WLS linearity #2 dark	38	DARK	L
77	WLS linearity #2	38	WLS	L
78	WLS linearity #3 dark	39	DARK	L
79	WLS linearity #3	39	WLS	L
80	WLS linearity #4 dark	40	DARK	L
81	WLS linearity #4	40	WLS	L
82	WLS linearity #5 dark	41	DARK	L
83	WLS linearity #5	41	WLS	L
84	WLS linearity #6 dark	42	DARK	L
85	WLS linearity #6	42	WLS	L
86	WLS linearity #7 dark	43	DARK	L
87	WLS linearity #7	43	WLS	L
88	WLS linearity #8 dark	44	DARK	L
89	WLS linearity #8	44	WLS	L
90	WLS linearity #9 dark	45	DARK	L
91	WLS linearity #9	45	WLS	L
92	WLS linearity #10 dark	46	DARK	L
93	WLS linearity #10	46	WLS	L
94	WLS linearity #11 dark	47	DARK	L
95	WLS linearity #11	47	WLS	L
96	LEO Dark,unbinned #1;exp.time 100	48	DARK	L
97	LEO Dark,unbinned #2;exp.time 500	49	DARK	L
98	LEO Dark,unbinned #3;exp.time 1000	50	DARK	L
99	LEO Dark,unbinned #4;exp.time 1500	51	DARK	L
100	LEO Dark,unbinned #5;exp.time 2000	52	DARK	L
101	LEO Dark,unbinned #6;exp.time 3000	53	DARK	L
102	LEO Dark,unbinned #7;exp.time 6000	54	DARK	L
103	LEO Dark;long exposure middle	55	DARK	L,D
104	WLS LEO radiometric dark	30	DARK	L
105	WLS LEO radiometric	30	WLS	L
106	WLS LEO stability BF4 dark	56	DARK	L
107	WLS LEO stability BF4	56	WLS	L
108	WLS LEO stability BF1 dark	57	DARK	L
109	WLS LEO stability BF1	57	WLS	L
110	LED LEO stability dark (60 sec)	31	DARK	L
111	LED LEO stability (60 sec)	31	LED	L
112	LED LEO stability BF4 dark	58	DARK	L
113	LED LEO stability BF4	58	LED	L
114	LED LEO stability BF1 dark	59	DARK	L
115	LED LEO stability BF1	59	LED	L
116	CTE long exposure long	60	DARK	L
117	Central Tropical Dark	61	DARK	L
118	Central Tropical	61	EARTH	L
119	Central Midlatitude Dark	62	DARK	L
120	Central Midlatitude	62	EARTH	L
121	Central Arctic Dark	63	DARK	L
122	Central Arctic	63	EARTH	L
123	Central Ozone Hole Dark	64	DARK	L
124	Central Ozone Hole	64	EARTH	L
125	Left Tropical Dark	65	DARK	L
126	Left Tropical	65	EARTH	L
127	Right Tropical Dark	66	DARK	L
128	Right Tropical	66	EARTH	L
129	Left Midlatitude Drak	67	DARK	L
130	Left Midlatitude	67	EARTH	L
131	Right Midlatitude Dark	68	DARK	L
132	Right Midlatitude	68	EARTH	L
133	Left Arctic Dark	69	DARK	L
134	Left Arctic	69	EARTH	L
135	Right Arctic Dark	70	DARK	L
136	Right Arctic	70	EARTH	L
137	Left Ozone Hole Dark	71	DARK	L
138	Left Ozone Hole	71	EARTH	L
139	Right Ozone Hole Dark	72	DARK	L
140	Right Ozone Hole	72	EARTH	L
141	Long Exposure Short Bad Pixels	73	DARK	D
142	Long Exposure Long Bad Pixels	74	DARK	D
143	WLS linearity #12 dark	75	DARK	L
144	WLS linearity #12	75	WLS	L
145	WLS linearity #13 dark	76	DARK	L
146	WLS linearity #13	76	WLS	L
147	LED linearity #1 dark	77	DARK	M1
148	LED linearity #1	77	LED	M1
149	LED linearity #2 dark	78	DARK	M1
150	LED linearity #2	78	LED	M1
151	LED linearity #3 dark	79	DARK	M1
152	LED linearity #3	79	LED	M1
153	LED linearity #4 dark	80	DARK	M1
154	LED linearity #4	80	LED	M1
155	LED linearity #5 dark	81	DARK	M1
156	LED linearity #5	81	LED	M1
157	LED linearity #6 dark	82	DARK	M1
158	LED linearity #6	82	LED	M1
159	LED linearity #7 dark	83	DARK	M1
160	LED linearity #7	83	LED	M1
161	LED linearity #8 dark	84	DARK	M1
162	LED linearity #8	84	LED	M1
163	LED linearity #9 dark	85	DARK	M1
164	LED linearity #9	85	LED	M1
165	LED linearity #10 dark	86	DARK	M1
166	LED linearity #10	86	LED	M1
167	LED linearity #11 dark	87	DARK	M1
168	LED linearity #11	87	LED	M1
169	LED linearity #12 dark	88	DARK	M1
170	LED linearity #12	88	LED	M1
171	LED linearity #13 dark	89	DARK	M1
172	LED linearity #13	89	LED	M1
173	LED linearity #14 dark	90	DARK	M1
174	LED linearity #14	90	LED	M1
175	LED linearity #15 dark	91	DARK	M1
176	LED linearity #15	91	LED	M1
177	LED linearity #16 dark	92	DARK	M1
178	LED linearity #16	92	LED	M1

UV1 and UV2 optics regions. For the calibration product, there is no such subchannel split.

Groundpixel flags are only available for the global and zoom-in radiance products and the statistics are calculated for UV1, UV2, and VIS.

For pixel and groundpixel-based statistics, only pixels are counted that are actually written to the measurement swaths in the output products, i.e., for radiance and irradiance products only the pixels in the so-called "optics region" taken into account. In the case of irradiance measurements, which are also written to the calibration product (this is the only type of measurement for which the calculation is split up into UV1 and UV2 subchannels for the calibration product), the UV1 and UV2 counts are merged (added up) into the UV pixel statistics before being written to the output product.

In case of rebinning in global radiance products (done for spatial zoom-mode earth measurements), pixel and groundpixel-based statistics are calculated on the rebinned pixels.

Measurements for which only calibration swaths (e.g., offset swath, spectral calibration swath) are written, are also taken into account for measurement-based statistics.

Raw measurements in the calibration product are not used in the calculation of the QA statistics.

VII. Conclusion

The OMI instrument produces large and complex Level 1b output products. In order to understand and use these products it is essential to understand the way OMI measurements are performed. For that purpose we have described in this paper the instrument operations concept, the way data processing is organized for OMI and, especially, which corrections are applied to the instrument data by the GDPS. These corrections have been related to a forward model of the signal flow through the instrument. An important, but unfortunately often ignored, aspect of the Level 1b data products is the information contained in the flags. A description is provided of the meaning of the various flags and the QA statistics entries in the metadata.

The OMI groundsegment has been operating successfully since launch. This is the result of extensive testing of both the software and the groundsegment as a whole.

The GDPS software will continue to evolve during the lifetime of the Aura mission but no major changes are anticipated.

Appendix

Table VII provides a summary of all Instrument Configurations (IcId) used by OMI, the related MeasurementClass, and the Orbit types in which these are used. The entry ELU refers to the electronic unit configuration. Instrument configurations with identical ELU numbers indicate are identical in terms of instrument readout but serve different purposes. For example ELU 1 corresponds to instrument configurations 0, 3, and 22. IcId 0 is the dayside measurement over the tropics, 3 and 22 are the corresponding dark current measurements with and without the Folding Mirror (FMM) in the optical light path. An L indicates that the instrument configuration was used during the Launch and Early Operations phase (first 90 days of the mission) to obtain in-flight calibration measurements. These configurations are not used during standard operations but can be scheduled when deemed necessary.

The order in which instrument configurations are used during the various types of orbits is indicated in Table VI. Time runs from top to bottom. Indicated are the times that the spacecraft enters and exits eclipse and spacecraft midnight. Level 1b data products cover the time between subsequent spacecraft midnights.

References

[1] P. F. Levelt *et al.*, "Science objectives of the Ozone Monitoring Instrument," *IEEE Trans. Geosci. Remote Sens.*, vol. 44, no. 5, pp. 1199–1208, May 2006.

[2] M. R. Dobber *et al.*, "Ozone Monitoring Instrument calibration," *IEEE Trans. Geosci. Remote Sens.*, vol. 44, no. 5, pp. 1209–1238, May 2006.

[3] P. F. Levelt *et al.*, "The Ozone Monitoring Instrument," *IEEE Trans. Geosci. Remote Sens.*, vol. 44, no. 5, pp. 1093–1101, May 2006.

[4] *Guide to Applying the ESA Software Engineering Standards to Small Software Projects*, May 1996. ESA, BSSC(96)2.

[5] *Release 6a SDP Toolkit Users Guide for the ECS Project*, Nov. 2003. Doc. 333-CD-600-001.

[6] *Input and Output Data Specification (IODS)*, Feb. 24, 2005. SD-OMIE-7200-DS-467.

G. H. J. van den Oord is currently with the Royal Dutch Meteorological Institute (KNMI), De Bilt, The Netherlands. He has a 16-year-long background in both observational and theoretical astrophysics with emphasis on solar and stellar magnetic activity. On the theoretical side, he has worked in the fields of magnetohydrodynamics, plasma physics, beam electrodynamics, high-energy astrophysics, X-ray spectroscopy, and radiative transport. On the observational side, he has been an active user of (ground-based) radio and optical instrumentation, and spaceborne X-ray and (E)UV instrumentation. He has supervised two Ph.D. students and is author and coauthor of 72 papers. Since April 1999, he has been the Deputy Principal Investigator of the Ozone Monitoring Instrument. He has been a Visiting Professor at the University of Catania. He has been a member of numerous science advisory boards on both national and international level.

Dr. van den Oord received an award from Utrecht University for outstanding research accomplishments.

Nico C. Rozemeijer received the B.Sc. degree in electrical engineering.

Since receiving his degree, he has worked as a Software Engineer on a broad range of projects. He is currently a Software Engineer with TriOpSys BV, Maarssen, The Netherlands, working on the OMI project since 2000.

V. Schenkelaars, photograph and biography not available at the time of publication.

Pieternel F. Levelt received the M.S. degree in physical chemistry and the Ph.D. degree from the Free University of Amsterdam, Amsterdam, The Netherlands, in 1987 and 1992, respectively. Her Ph.D. work consisted of the development of a XUV spectrometer-based nonlinear optical technique and performing XUV spectroscopy on small diatomic molecules.

In 1993, she started working at the Royal Netherlands Meteorological Institute (KNMI), De Bilt, in the Atmospheric Composition section at the Research Department of KNMI. There, she worked on chemical data assimilation of ozone in two-dimensional and three-dimensional chemistry transport models and on the validation of the European satellite instruments GOME and SCIAMACHY. She was a Member of the Algorithm and Validation subgroups of GOME and SCIAMACHY. She was strongly involved in the validation program of both instruments. Since July 1998, she has been Principal Investigator of the OMI instrument and is responsible for the scientific program of OMI and managing the international OMI Science Team. She is also the Project Manager of the OMI Program at KNMI and responsible for the development of algorithms, validation, and data processing of OMI products and in-flight calibration and operational planning of the OMI instrument. She is managing the OMI team at KNMI consisting of 15 to 35 people. As Principal Investigator, she is advising NIVR on OMI instrument requirements and performance.

Marcel R. Dobber studied experimental physics from 1990 to 1994 at the Free University of Amsterdam, Amsterdam, The Netherlands, and received the Ph.D. degree in physical chemistry from the University of Amsterdam, for work on high-resolution and time-resolved molecular laser spectroscopy.

He started working on Earth observation from space in 1995 and joined the Royal Dutch Meteorological Institute (KNMI), De Bilt, The Netherlands, in 2001, where he has been working mainly on the development and on-ground and in-flight calibration of the OMI instrument on NASA's EOS Aura satellite.

Robert H. M. Voors received the M.Sc. degree in astrophysics and the Ph.D. degree from Utrecht University, Utrecht, The Netherlands, in 1994, in 1994 and 1999, respectively. His Ph.D. thesis was for his study of the evolution of the most massive stars.

He went to work at the Royal Netherlands Meteorological Institute (KNMI), De Bilt, for the OMI project in 1999, first on the development of retrieval algorithms, and later on the in-flight calibration of OMI.

J. Claas, photograph and biography not available at the time of publication.

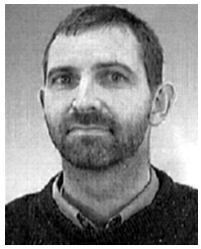

Johan de Vries has over 15 years of experience in developing spectrographs for space. He has acted as OMI Project Scientist on the industrial side from 1994 up to launch on EOS Aura in 2004. He is currently a Design Leader for future air quality instruments at Dutch Space BV, Leiden, The Netherlands.

M. ter Linden, photograph and biography not available at the time of publication.

C. De Haan, photograph and biography not available at the time of publication.

T. van de Berg, photograph and biography not available at the time of publication.